

## TOWARD TW-LEVEL, HARD X-RAY PULSES AT LCLS\*

W.M. Fawley<sup>1</sup>, J. Frisch<sup>1</sup>, Z. Huang<sup>1</sup>, Y. Jiao<sup>1</sup>, H.-D. Nuhn<sup>1</sup>, C. Pellegrini<sup>1,2</sup>, S. Reiche<sup>3</sup>, J. Wu<sup>1†</sup>

<sup>1</sup>SLAC National Accelerator Laboratory, Menlo Park, CA 94025, USA

<sup>2</sup>Department of Physics and Astronomy, UCLA, Los Angeles, CA 90095-1547, USA

<sup>3</sup>Paul Scherrer Institute, Villigen PSI, 5232, Switzerland

### Abstract

Coherent diffraction imaging of complex molecules such as proteins requires a large number (*e.g.*,  $\sim 10^{13}$ /pulse) of hard X-ray photons within a time scale of  $\sim 10$  fs or less. This corresponds to a peak power of  $\sim 1$  TW, much larger than that currently generated by LCLS or other proposed X-ray free electron lasers (FELs). We study the feasibility of producing such pulses using a LCLS-like, low charge electron beam, as will be possible in the LCLS-II upgrade project, employing a configuration beginning with a SASE amplifier, followed by a “self-seeding” crystal monochromator [1], and finishing with a long tapered undulator. Our results suggest that TW-level output power at 8.3 keV is possible from a total undulator system length around 200 m. In addition power levels larger than 100 GW are generated at the third harmonic. We present a tapering strategy that extends the original “resonant particle” formalism by optimizing the transport lattice to maximize optical guiding and enhance net energy extraction. We discuss the transverse and longitudinal coherence properties of the output radiation pulse and the expected output pulse energy sensitivity, both to taper errors and to power fluctuations on the monochromatized SASE seed.

### Introduction

LCLS is presently the brightest source of coherent X-rays, producing pulses of about  $10^{12}$ , 0.5 to 9-keV photons in 70 to 100 fs, and pulses shorter than 10 fs at reduced intensity [2, 3]. Its peak power and brightness are about ten orders of magnitude larger than any existing synchrotron light source. The very short and extremely bright LCLS X-ray pulses are being used to explore many new areas of science. One very interesting biological application is obtaining a single diffraction pattern from a large macromolecule, such as a virus or a single cell, before the sample explodes into a plasma. LCLS’s unique capabilities have been successfully used recently to obtain coherent diffraction images both of proteins in nano-crystals [4] and of a virus [5]. The nano-crystal imaging experiment used 70-fs long pulses of about  $10^{12}$  photons at 1.8 keV energy. Diffraction peaks from these data were identified, indexed and combined into a set of 3D structure factors. Reducing the pulse duration to 10 fs or less and simultaneously increasing the number of photons to about  $10^{13}$  at 8-10 keV

photon energies would allow measurements of even smaller nano-crystals, down to a single molecule. These parameters correspond to an instantaneous power of TW.

The scientific interest of reaching this goal has led us to begin study of the feasibility of obtaining TW-level output pulses with LCLS-like electron beam parameters. The underlying method chosen to reach TW powers is that proposed by Kroll, Rosenbluth, and Morton (KMR) [6] to increase the energy transfer from the electrons to radiation by adjusting the undulator magnetic field to compensate for the electron energy losses, a “tapered” undulator. The initial results are reported here.

### Tapering Strategy

As is well known and experimentally verified, high gain, single pass FEL amplifiers reach saturation at a power level of  $P_{\text{sat.}} \sim \rho P_{\text{beam}}$  where  $P_{\text{beam}}$  is the electron beam power and  $\rho$  is the FEL efficiency parameter [7]. This behavior is true for both SASE and externally-seeded configurations and arises from the growth of instantaneous energy spread and the rotation of the microbunched electrons in the ponderomotive well formed by the FEL radiation and the undulator magnetic field. For electron beam parameters corresponding to the proposed LCLS-II project at SLAC,  $\rho \sim 5 \times 10^{-4}$ , the nominal saturation power is  $\sim 30$  GW, far below the TW level. However, near and at saturation the microbunching fraction is large (bunching factor:  $b_1 \sim 0.5$ ) suggesting that with proper tapering of the normalized undulator strength  $K$ , one can both trap and then decelerate a comparable fraction of the electrons to extract much greater additional power [6]. For example, currently LCLS doubles its output power to  $\sim 70$  GW using its available tapering range of  $\Delta K/K \sim 0.8\%$ .

The proposed LCLS-II undulators will have fully tunable gaps and in principle can taper  $K$  fully to zero. Moreover, there is currently great interest in giving LCLS-II a self-seeding option employing the crystal monochromator scheme [1]. With respect to energy extraction via tapering and thus required undulator length, the nearly monochromatic radiation field produced by self-seeding is very attractive because the stochastic nature of SASE temporal profile prevents a more aggressive taper [8] from reaching very high power. Consequently, our preliminary design for an 8.3-keV, TW-level FEL starts with a SASE undulator sufficiently long to generate GW-level radiation. This radiation then passes through a crystal monochromator that results in a MW-level, nearly monochromatic wake. At the same longitudinal location, the electron bunch passes

\* Work supported by U.S. Department of Energy, Office of Basic Energy Sciences, under Contract DE-AC02-76SF00515. This work was performed in support of the LCLS project at SLAC.

† Corresponding author: jhwu@SLAC.Stanford.EDU

through a gentle four-dipole chicane that provides: 1. a time-delay for temporal overlap with the monochromatic wake; 2. a transverse offset to pass around the crystal; and 3. a temporal smearing of the microbunching developed in the SASE undulator section. Following the chicane, the radiation and electron beam enter a second undulator in which first the radiation grows exponentially to saturation and then, via a tapering of  $K$  to maintain a high electron microbunching fraction, continues to strongly grow to TW power levels. A similar study on TW power levels from the European XFEL has been previously conducted [9].

We have examined two possible tapering strategies. The first uses the “standard” KMR formulation [6] in which a virtual design electron is maintained at a synchronous phase  $\psi_r$  while its energy  $\gamma_r mc^2$  decreases at a rate  $\propto \tilde{E} \sin \psi_r$  where  $\tilde{E}$  is the slowly varying FEL electric field. As shown by KMR, maximizing the product of the area of ponderomotive well and  $\sin \psi_r$  occurs at  $\psi_r \approx 0.45$ . A self-design taper algorithm based upon the KMR formalism has been implemented in the GINGER simulation code [10] where  $\tilde{E}$  and  $K(z)$  are calculated self-consistently. While this approach typically keeps the trapped particle fraction  $f_T$  nearly constant with decreasing  $K$ , it does not necessarily maximize the power at any given  $z$ .

Our second approach [11] was to develop empirically optimized  $K(z)$  tapers that maximize the output power at a fixed total undulator length without necessarily trying to keep  $f_T$  large at undulator exit. Let us start with some discussion on scaling laws for the  $z$ -behavior of  $\tilde{E}$  and thus  $K$ . For a well-designed taper configuration where both  $f_T$  and mean ponderomotive phase of the trapped electrons stay roughly constant and diffraction effects remain small (*e.g.* due to gain and/or refractive optical guiding),  $\tilde{E}$  should grow linearly and thus radiation power quadratically with  $z$ . From energy conservation, the mean energy loss  $\Delta\gamma$  of the trapped electrons must also change quadratically with  $z$  and, to maintain the FEL resonance condition, we expect  $K(z) \approx K_0 \times [1 - a(z - z_0)^2]$ , where  $a > 0$  characterizes the taper rate and  $z_0$  is the taper start location (nominally close to the end of the exponential gain in the second undulator). Eventually though, due to the weakening of optical guiding as the radiation electric field increases,  $\tilde{E}(z)$  approaches an asymptotic constant and the radiation power then grows only linearly. This requires a linear tapering, *i.e.*,  $dK(z)/z \sim \text{constant}$ , and also that the FEL mode size  $\sigma_r$  grows as  $\sqrt{z}$ . With these two limiting cases in mind, we propose a more general and empirical method to formulate a mathematical function  $K(z) = K_0[1 - a(z - z_0)^b]$ , with  $b$  not necessarily an integer, so that  $[\tilde{E}(z)/\tilde{E}(z_0)] \sin \psi_r \approx -CdK(z)/dz = abC(z - z_0)^{b-1}$  [6], with  $C > 0$  being approximately constant. This formula indicates that  $b > 1$  is necessary for  $\tilde{E}$  increasing with  $z$  if  $\psi_r$  is constant.

We have also considered a  $z$ -dependent optimization of the electron beam transverse size for better coupling to the radiation mode size. In the exponential growth regions of high gain amplifiers, gain guiding minimizes diffraction effects and generally strong external focusing on the electron

beam will minimize the gain length. However, in the tapered region well beyond initial saturation, gain guiding becomes much weaker, the radiation transverse size starts to increase, and it is no longer clear that the strong focusing parameters chosen for the exponential gain region remain optimum. Hence, we separate the post-monochromator undulator into a stepwise optimization of the transverse electron beam focusing strength. This helps to improve the trapping efficiency and thus the power output. The optimization package optimizes FEL output power with respect to the above mentioned parameters:  $a$ ,  $b$ ,  $z_0$ , and the transverse focusing; fuller detail and the underlining physics will be presented elsewhere [11]. Note that this approach does not explicitly specify a synchronous phase  $\psi_r$ , although at any given  $z$  there is such a phase for which a virtual particle at resonant energy will maintain constant ponderomotive phase as it decelerates. To minimize computational expense, optimization is done with the GENESIS code [12] in time-steady mode, followed by fine tuning with full time-dependent runs to get better performance.

### An 8.3-keV, TW FEL for LCLS-II

Our study adopted the following LCLS-II electron beam and undulator parameters. The e-beam has bunch charge  $Q = 40$  pC, a Gaussian longitudinal profile with peak current  $I_{pk} = 4$  kA, mean energy  $E_0 = 13.64$  GeV, relative incoherent rms energy spread  $\sigma_\delta = 1.0 \times 10^{-4}$ , and normalized transverse emittance  $\varepsilon_n = 0.3$  mm-mrad for both  $x$ - and  $y$ -planes. The undulator has period  $\lambda_w = 3.2$  cm, and is composed of 3.4-m long sections separated by 1-m breaks for focusing and diagnostics. The nominal average  $\beta$ -function is 20 m for both  $x$ - and  $y$ -planes.

The system design starts with an 8.3-keV, SASE FEL reaching 1-GW power level in a total length of  $\sim 30$  m. The electron bunch then passes through a 3.4 m long chicane whose nominal  $R_{56} = 12 \mu\text{m}$  delays the electron bunch by 20 fs with respect to the photon beam. The SASE output radiation traverses a single crystal, diamond monochromator with Bragg surface C(400) and thickness of 100  $\mu\text{m}$ . The resulting, nearly monochromatic seed with  $P \approx 5$  MW then recombines with the electron bunch at the entrance of the second undulator. The second undulator, with identical period and section lengths as the first and a total length of 160 m, then amplifies the radiation to TW levels.

**System optimization, scaling, and sensitivity** – As explained above, we optimized our taper design via time-steady GENESIS simulations. The optimization package found a taper that begins at  $z_0 \approx 16$  m with the taper power exponent of  $b = 2.03$ , very close to quadratic tapering. For a total taper of 13 %, the optimized power for a 200-m undulator length was  $\approx 2.7$  TW. The power evolution along the undulator is shown as the red curve in Fig. 1. For comparison, a KMR-style taper using GINGER gives 2.3 TW but with a residual trapped fraction of  $\approx 0.45$ .

Postponing temporarily discussion of important side-band effects, we also explored the scaling of such a TW

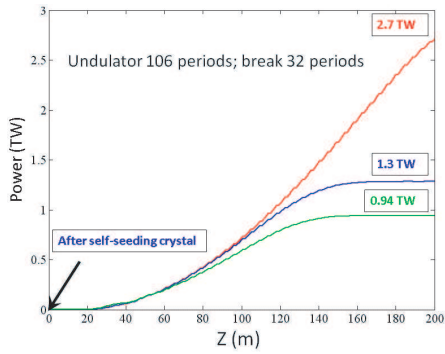


Figure 1: GENESIS predictions for amplification of a 5-MW seed in a tapered, 200-m long undulator for time-steady (red), full time-dependent “fresh” bunch (blue), and start-to-end (green) conditions.

FEL on various parameters. Simulation confirmed that FEL power scales quadratically with current, as one would expect for coherent emission from a highly microbunched electron bunch. The requirement on the emittance is relatively loose in the tapered region compared to the exponential growth region. We found that for the above parameter set, emittances as large as  $\varepsilon_n = 0.4$  mm-mrad can still produce TW-level output within similar total undulator system length. Due to an energy-spread induced smearing effect on the microbunching factor in break sections, a short break distance is also favored. The dependence of output power upon the input seed level is also very relevant because the nominal, single mode output of self-seeding scheme will have large shot-to-shot fluctuations. Figure 2 displays output power at  $z = 160$  m as a function of input seed power  $P_I$ ; one sees little sensitivity for  $P_I \geq 1$  MW. For a negative exponential input power distribution with  $\langle P \rangle = 5$  MW, the RMS output fluctuation level grows from  $\approx 6\%$  at the beginning of the tapered region to about 17% by  $z = 160$  m. By designing the taper for a somewhat smaller seed power (e.g., 3 MW), the fluctuation level can be reduced at the expense of partially reduced output power. Our results also suggest a TW FEL based on a tapered undulator is more sensitive to undulator section tuning errors than is an untapered FEL. For a random, uncorrected section  $K$ -error with rms  $\sigma_{\Delta K/K} \sim 10^{-4}$ , our nominal design shows a 15% reduction in power. The same error level in an untapered undulator produces a 3.5% reduction of the power at saturation.

**Sideband Instability Effects** – We now turn to time-dependent effects. Because our design utilizes a long undulator after the self-seeding crystal, even though the seed is much stronger compared to the shot-noise in the electron beam, the SASE components originating from shot noise on the electron bunch can excite the sideband instability in the tapered region [6, 13]. Furthermore, while the chicane between the two undulators smears out the energy and density microbunching at x-ray wavelength scales arising from the first SASE undulator, in general it will *not* smear

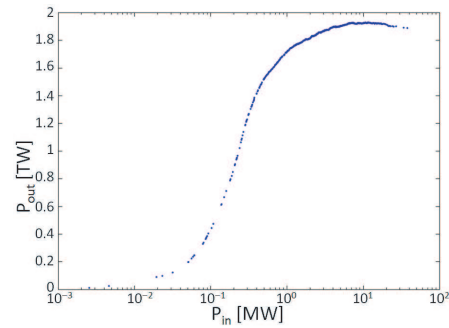


Figure 2: Sensitivity of final FEL power at 160 m as a function of the monochromatized, input seed power as predicted by time-steady GENESIS simulation.

out longer scale (*i.e.*, at the coherence length) modulations induced by the SASE process. In fact, the chicane  $R_{56}$  will induce a current modulation [14] from longer wavelength, SASE energy modulations. This modulation both will broaden the bandwidth of the FEL radiation in the exponential gain region of the second undulator, and, more importantly, also provide an additional seed for the sideband instability in the tapered region at a level much above that corresponding to random shot noise. To distinguish this additional seed effect, we simulate a “fresh” bunch scheme as compared to the start-to-end simulation.

Assuming that we start the second undulator simulation with a “fresh” electron bunch to interact with the monochromatized seed. The full time-dependent simulation shows power saturation at 1.3 TW (see the blue curve in Fig. 1) or less than half the power predicted by time-steady results. It appears the early saturation arises from strong, sideband-induced detrapping from the ponderomotive wells; Fig. 3 shows significant temporal modulation in the radiation power by  $z = 160$  m. Surprisingly, the spectrum remains quite good as shown in Fig. 4. The bandwidth is about twice the transform limit for the macroscopic current profile. Transversely, about 80% of the total power resides in the fundamental TEM00 Gaussian mode and the overall transverse coherence is quite good ( $M^2 \sim 1.3$ )<sup>1</sup>.

In contrast, in the start-to-end simulation, we start the second undulator simulation with the same electron bunch which has experienced the SASE FEL in the first undulator as well as the smearing process in the chicane. In our case, when the SASE FEL reaches 1 GW, the fundamental microbunching fraction  $b_1 \approx 0.1$ . After the chicane, the microbunching is smeared out by more than one order of magnitude to a reduced bunching factor of  $b_1 \approx 0.008$ . At the end of the SASE FEL, on average the SASE spikes develop a relative rms energy spread  $\sigma_\delta \sim 2.0 \times 10^{-4}$ . Given the chicane momentum compaction factor of  $R_{56} = 12$   $\mu$ m, the rms pathlength change  $\sigma_{\Delta L} \sim 2.7$  nm. Consequently, the chicane strongly washes out energy and density modulations only within length scales shorter than  $2\pi \sigma_{\Delta L}/\lambda_r \sim 100$  radiation periods. On the other hand,

<sup>1</sup>Following an approach of G. Penn at LBL.

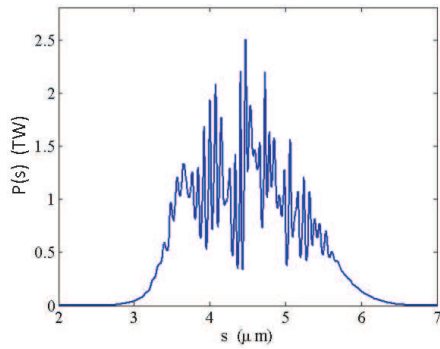


Figure 3: The instantaneous, 8.3-keV power profile at  $z = 160$  m in the second undulator according to time-dependent GENESIS simulation.

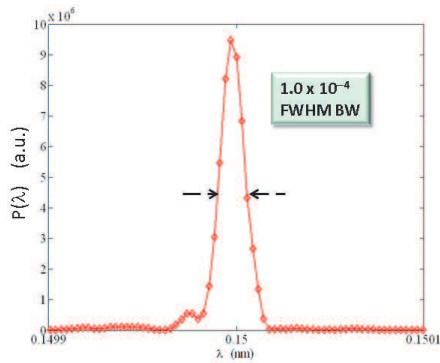


Figure 4: The radiation spectrum profile at 160 m corresponding to the previous figure.

the synchrotron sideband modulation length is on the order of  $\lambda_r/4\rho \sim 300\lambda_r$  [13]. Therefore, SASE components at this wavelength will be little damped and will excite the sideband instability. Such start-to-end simulation shows that the FEL power will saturate at 0.94 TW, about 30% lower than the simulation with “fresh” electron bunch as shown in Fig. 1 as the green curve.

**Harmonic Emission** – The large bunching factor in the tapered portion of the second undulator leads to significant nonlinear harmonic generation (presuming a planar undulator). For an example with the same e-beam parameters as before but with shorter undulator break sections (about 0.3 m), time-steady simulation shows that the 3<sup>rd</sup> harmonic (25-keV photon energy) power can reach  $\approx 10\%$  that of the fundamental or nearly 1 TW for this particular case (see Fig. 5). This fraction is much larger than normally found at saturation for high gain amplifiers and appears to be due to a quite high  $b_3 \geq 0.2$  in the tapered region; similar GINGER simulations confirm this and also find 5<sup>th</sup> harmonic emission at the 0.3% level of the fundamental.

## Conclusion

Our simulation studies suggest that it is feasible with LCLS-like electron beam parameters to generate coherent, TW-level, hard x-ray pulses within a  $\sim 200$ -m

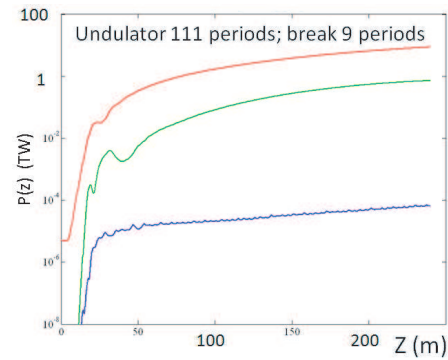


Figure 5: Fundamental (red), 2nd (blue), and 3rd (green) harmonic radiation power vs.  $z$  in an undulator with short break lengths.

long, tapered undulator system. Together with output at the fundamental resonant wavelength, there will also be strong ( $P_3 \geq 100$  GW) 3rd harmonic emission for planar-polarized undulators. To further improve the performance and shorten the undulator length, one can adopt helical undulator, while the study in this paper is for planar undulator. Furthermore, decreasing the break length between the undulator magnetic sections will naturally enhance the continuation of FEL power growth. To generate longer FEL pulse, one can adopt two-bunch self-seeding scheme with a 4-bend crystal monochromator working in the Bragg reflection configuration. The authors are pleased to thank E. Allaria, Y. Cai, A.W. Chao, Y. Ding, P. Emma, and G. Penn for many stimulating discussions.

## REFERENCES

- [1] G. Geloni, V. Kocharyan, and E. Saldin, DESY 10-053.
- [2] P. Emma *et al.*, Nature Photonics **4**, 641 (2010).
- [3] Y. Ding *et al.*, Part. Acc. Conf., p. 300, 2009; Y. Ding *et al.*, Phys. Rev. Lett. **102**, 254801 (2009).
- [4] H. N. Chapman *et al.*, Nature **470**, 73 (2011).
- [5] M. M. Seibert *et al.*, Nature **470**, 78 (2011).
- [6] N.M. Kroll, P.L. Morton, and M.N. Rosenbluth, IEEE J. Quantum Electronics, **QE-17**, 1436 (1981).
- [7] R. Bonifacio, C. Pellegrini, and L.M. Narducci, Opt. Commun., **50**, 373 (1984).
- [8] W.M. Fawley, Z. Huang, K.-J. Kim, and N.A. Vinokurov, Nucl. Instrum. Methods **A 483**, 537 (2002).
- [9] G. Geloni, V. Kocharyan, and E. Saldin, DESY 10-108.
- [10] W.M. Fawley, Nucl. Instrum. Methods **A 375**, 550 (1996).
- [11] Y. Jiao *et al.*, in preparation.
- [12] S. Reiche, Nucl. Instrum. Methods **A 429**, 243 (1999).
- [13] Z. Huang and K.-J. Kim, Nucl. Instrum. Methods **A 483**, 504 (2002).
- [14] E. A. Schneidmiller and M. V. Yurkov, Phys. Rev. ST Accel. Beams **13**, 110701 (2010).